Electronic Supplementary Material (ESI) for Dalton Transactions.

Two-dimensional magnetic behaviour in hybrid NiFe-layered double hydroxides by molecular engineering

Alvaro Seijas-Da Silva, [a] Jose Alberto Carrasco [a], Bruno J. C. Vieira [b], João C. Waerenborgh [b], Eugenio Coronado [a]*, Gonzalo Abellán [a]*

[a] Instituto de Ciencia Molecular (ICMol), Universidad de Valencia, Catedrático José Beltrán Martínez, 2, 46980 Paterna, Spain.
[b] Centro de Ciências e Tecnologias Nucleares (C2TN), Instituto Superior Técnico, Universidade de Lisboa, 2695-066 Bobadela LRS, Portugal.

Experimental part.

Anion exchange reaction.

Synthesis of NiFe-SO_4 LDH.
Sodium sulphate (0.25 M) was dissolved in 50 mL of a 1:1 (v/v) ethanol/water mixture with magnetic stirring at 65 °C and under argon atmosphere. After 30 min, 50 mg of LDH NiFe−Cl were added. The temperature was set at 50 °C, and the reaction was kept for 48 h. Finally, the mixture was filtered, washed with Milli-Q water and EtOH, and dried in vacuum.

Synthesis of NiFe-ES LDH.
Sodium ethyl sulphate (ES; 7.5 mM) was dissolved in 50 mL of a 1:1 (v/v) ethanol/water mixture. Then, 50 mg of NiFe−Cl LDH were added, and the reaction was maintained for 48 h at room temperature under Ar atmosphere and magnetic stirring. Finally, the final mixture was filtered, and the yellow powder was washed with Milli-Q water and EtOH several times and dried during 24 h in vacuum.

Synthesis of NiFe-OS LDH.
Sodium octyl sulphate (OS; 7.5 mM) was dissolved in 50 mL of a 1:1 (v/v) ethanol/water mixture. Then, 30 mg of NiFe−Cl LDH were added, and the reaction was maintained for 48 h at room temperature under Ar atmosphere and magnetic stirring. Finally, the final mixture was filtered, and the yellow powder was washed with Milli-Q water and EtOH several times and dried during 24 h in vacuum.

Synthesis of NiFe-DS LDH.
Sodium dodecyl sulphate (DS; 0.1 M) was dissolved in 50 mL of a 1:1 (v/v) ethanol/water mixture. Then, 200 mg of NiFe−Cl LDH were added, and the reaction was maintained for 12 h at room temperature under Ar atmosphere and magnetic stirring. Finally, the final mixture was filtered, and the yellow powder was washed with Milli-Q water and EtOH several times and dried during 24 h in vacuum.

Synthesis of NiFe-HDS LDH.
Sodium hexadecyl sulphate (HDS; 2.5 mM) was dissolved in 50 mL of a 1:1 (v/v) ethanol/water mixture. Then, 50 mg of NiFe−Cl LDH were added, and the reaction was maintained for 12 h at room temperature under Ar atmosphere and magnetic stirring. Finally, the final mixture was filtered, and the yellow powder was washed with Milli-Q water and EtOH several times and dried during 24 h in vacuum.

Synthesis of NiFe-ODS LDH.
Sodium octadecyl sulphate (ODS; 0.01 M) was dissolved in 50 mL of a 1:1 (v/v) ethanol/water mixture. Then, 200 mg of NiFe−Cl LDH were added, and the reaction was maintained for 12 h at room temperature under Ar atmosphere and magnetic stirring. Finally, the final mixture was filtered, and the yellow powder was washed with Milli-Q water and EtOH several times and dried during 24 h in vacuum.

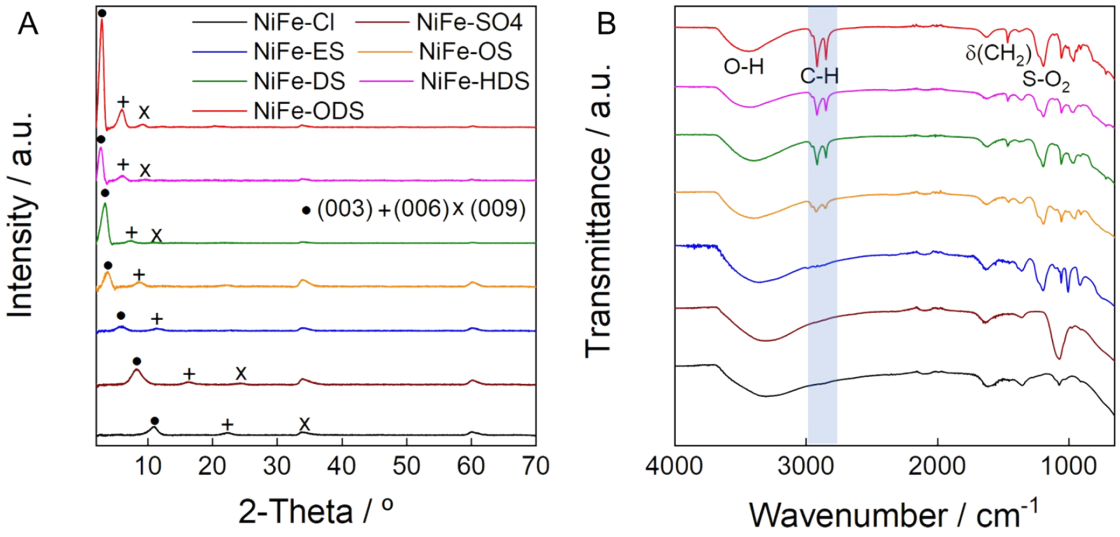

Figure S1. (A) XRPD diffractograms highlighting the main basal reflections and (B) IR spectra of the NiFe–LDH family.

LDH phases were confirmed via XRPD pattern, highlighting the main basal reflections that can be found in hydrotalcite-like materials (JCPDS 22-700).[1] The main (003), (006) and (009) peaks are related to the basal space of the LDH, hence dependent on the size of the interlayer anion. These peaks exhibit a shift towards lower 2-θ values as long as the length of the interlayer anion rises, indicative of a larger interlayer space.[2] At the same time, when the length of the interlayer surfactant rises, the intensity of these peaks increases due to a greater ordering in the c axis direction corresponding to a higher number of tail to tail interactions, which favours the stabilization of the system.[3,4] For the pristine NiFe-Cl, we observe a basal space of around 8.0 Å, in good agreement with that found in the literature.[2] For the longest interlayer distance (NiFe-ODS) the basal space increases up to 31.6 Å, confirming the successful anion exchange reaction.[4]

ATR-FTIR spectroscopy also confirm the nature of the interlayer anion, highlighting the C–H stretching bands at 2917 and 2845 cm^{-1} and the sulphate bands at ca. 1190 and 1050 cm^{-1} in the surfactant-intercalated samples and at ca. 1100 cm^{-1} in the sulphate sample.[5]

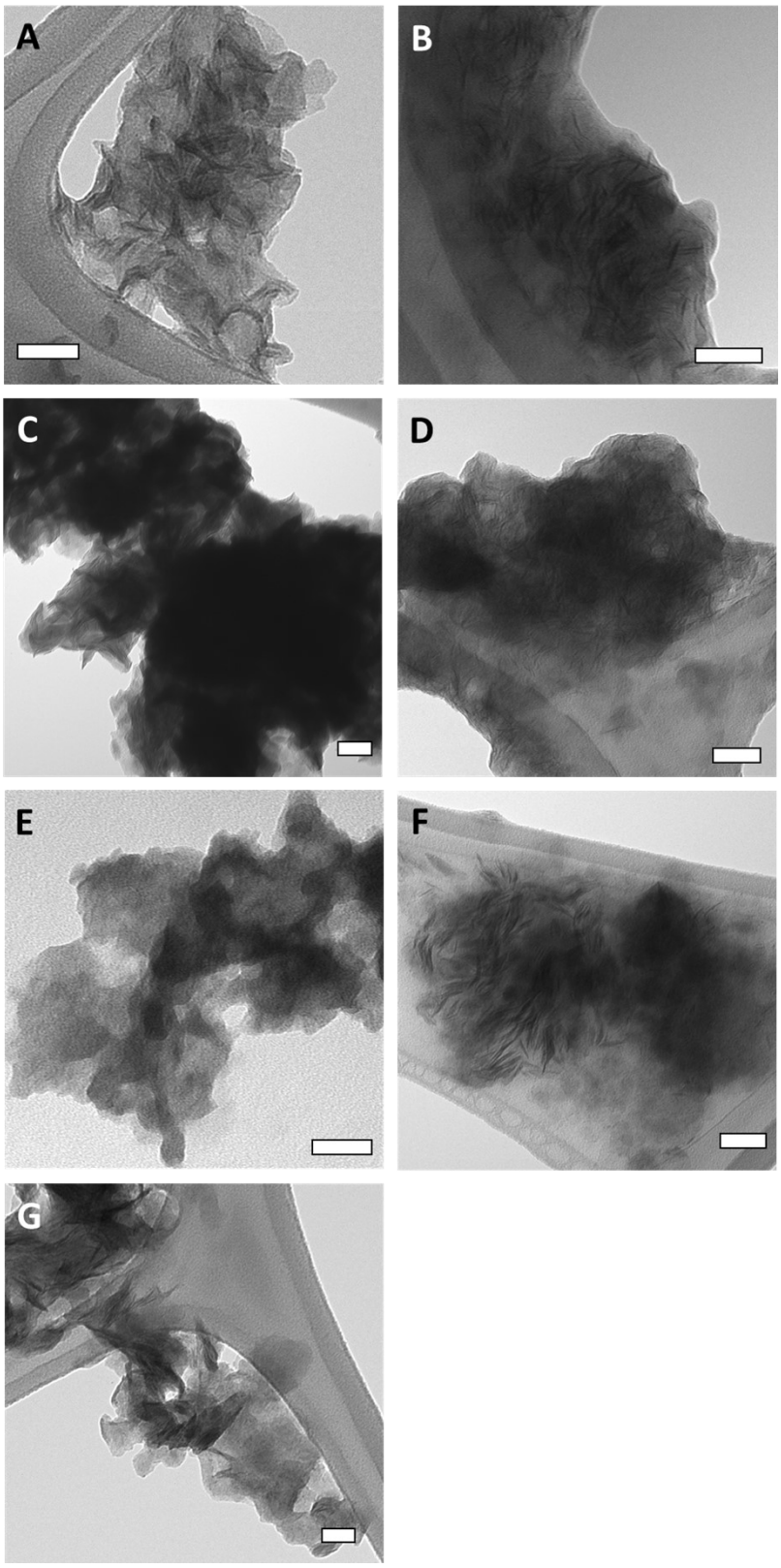

Figure S2. TEM images of the NiFe-LDHs. A) NiFe-Cl, B) NiFe-SO4, C) NiFe-ES, D) NiFe-OS, E) NiFe-DS, F) NiFe-HDS and G) NiFe-ODS. Scale bar: 50 nm.

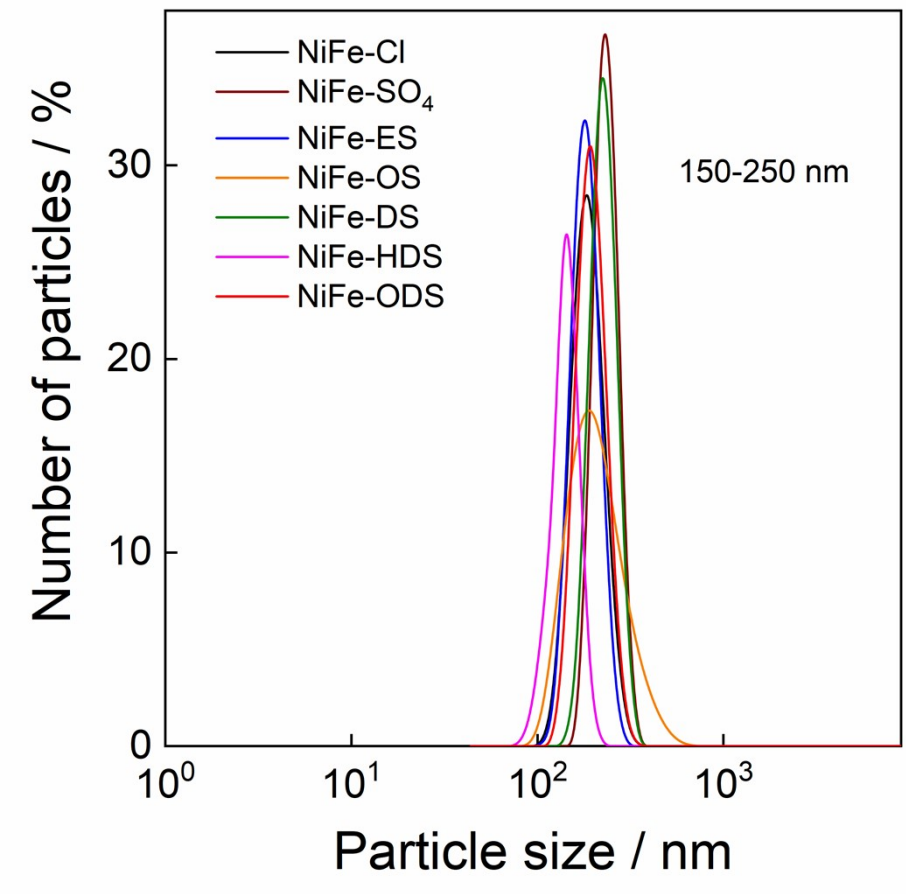

Figure S3. DLS measurements of NiFe-LDH family denoting the average size of the particles.

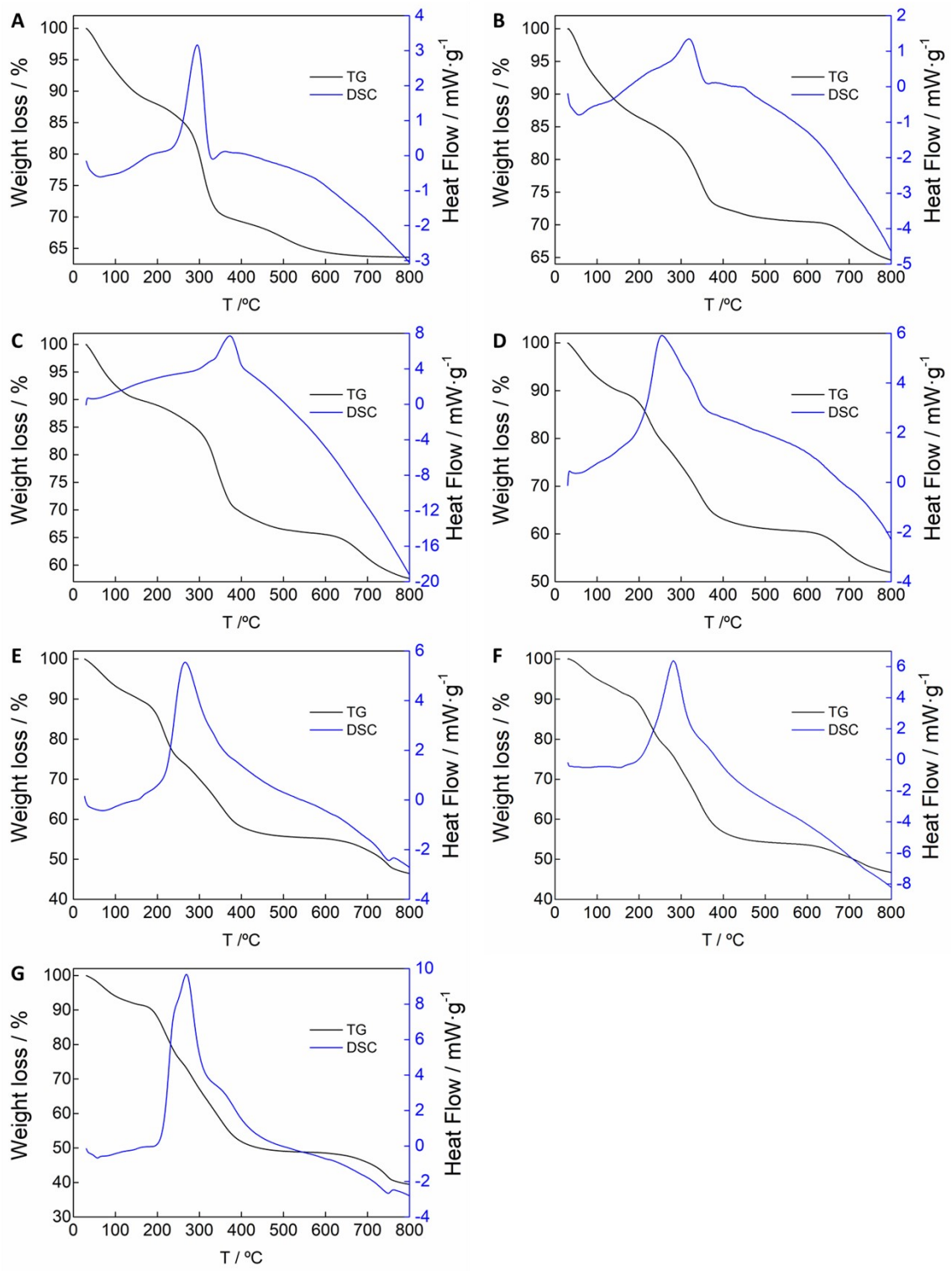

Figure S4. Thermogravimetric analysis for the as-synthesized LDHs. A) NiFe-Cl, B) NiFe-SO4, C) NiFe-ES, D) NiFe-OS, E) NiFe-DS, F) NiFe-HDS and G) NiFe-ODS.

Table S1. Elemental analysis of NiFe–LDH family and metallic ratio by EDX.

Sample	C_{found}	H_{found}	N_{found}	S_{found}	$C_{calculated}$	$H_{calculated}$	$N_{calculated}$	$S_{calculated}$	Ratio Ni/Fe
NiFe–Cl	3.24	3.32	0.65	0.17	3.29	3.21	0.00	0.00	2.73
NiFe–SO_4	5.20	3.34	0.42	2.98	5.14	3.37	0.00	3.56	2.75
NiFe–ES	6.60	3.63	0.59	3.42	6.68	3.66	0.00	4.09	2.68
NiFe–OS	13.01	4.34	0.56	3.84	13.09	4.53	0.00	4.36	2.85
NiFe–DS	19.26	5.30	0.34	3.85	19.46	5.38	0.00	4.33	2.74
NiFe–HDS	23.49	5.57	0.35	3.52	23.70	5.87	0.00	3.95	2.81
NiFe–ODS	27.44	6.33	0.32	3.45	27.01	6.73	0.00	3.65	2.86

Note: the calculated data correspond to the estimated molecular formulas.

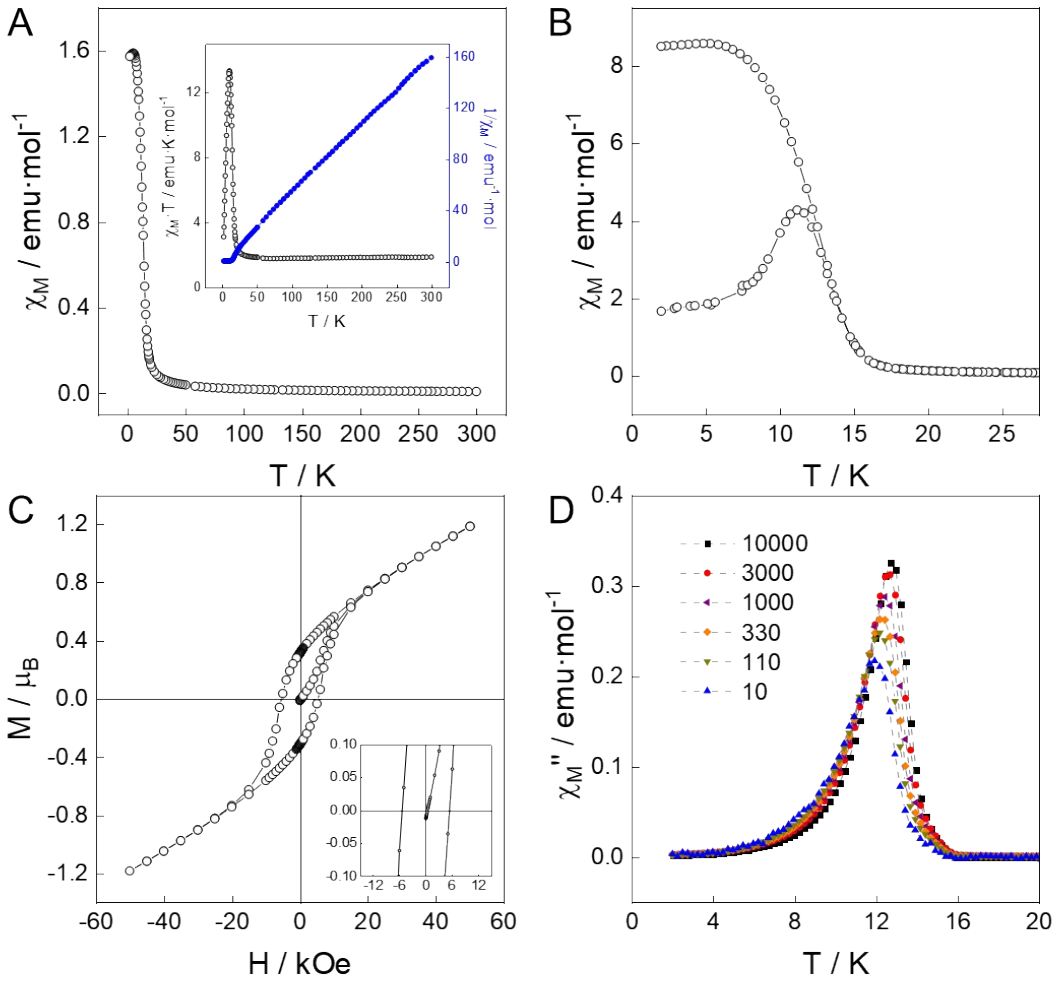

Figure S5. Magnetic properties of the NiFe-SO_4 sample. (A) χ_M vs. T with an external applied field of 1000 Oe. The inset represents the thermal dependence of $\chi_M \cdot T$ and the fitting of the χ_M^{-1} to a Curie–Weiss law; (B) FC/ZFC with an external applied field of 100 Oe. (C) Hysteresis cycle at 2 K. The inset shows a zoom of the low field region; (D) frequency dependence with the temperature for the out-of-phase (χ_M") signals at 10, 110, 330, 1000, 3000 and 100000 Hz.

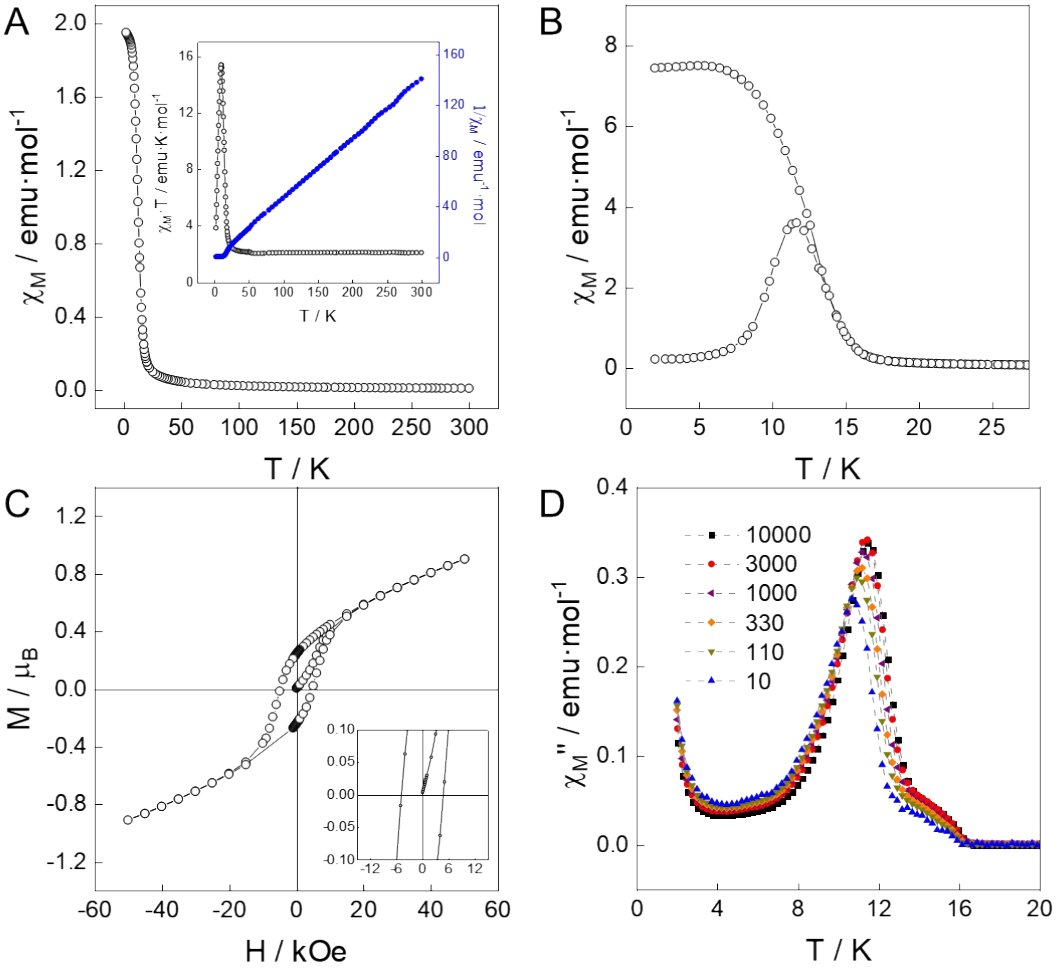

Figure S6. Magnetic properties of the NiFe-ES sample. (A) χ_M vs. T with an external applied field of 1000 Oe. The inset represents the thermal dependence of χ_M·T and the fitting of the χ_M^{-1} to a Curie–Weiss law; (B) FC/ZFC with an external applied field of 100 Oe. (C) Hysteresis cycle at 2 K. The inset shows a zoom of the low field region; (D) frequency dependence with the temperature for the out-of-phase (χ_M") signals at 10, 110, 330, 1000, 3000 and 100000 Hz.

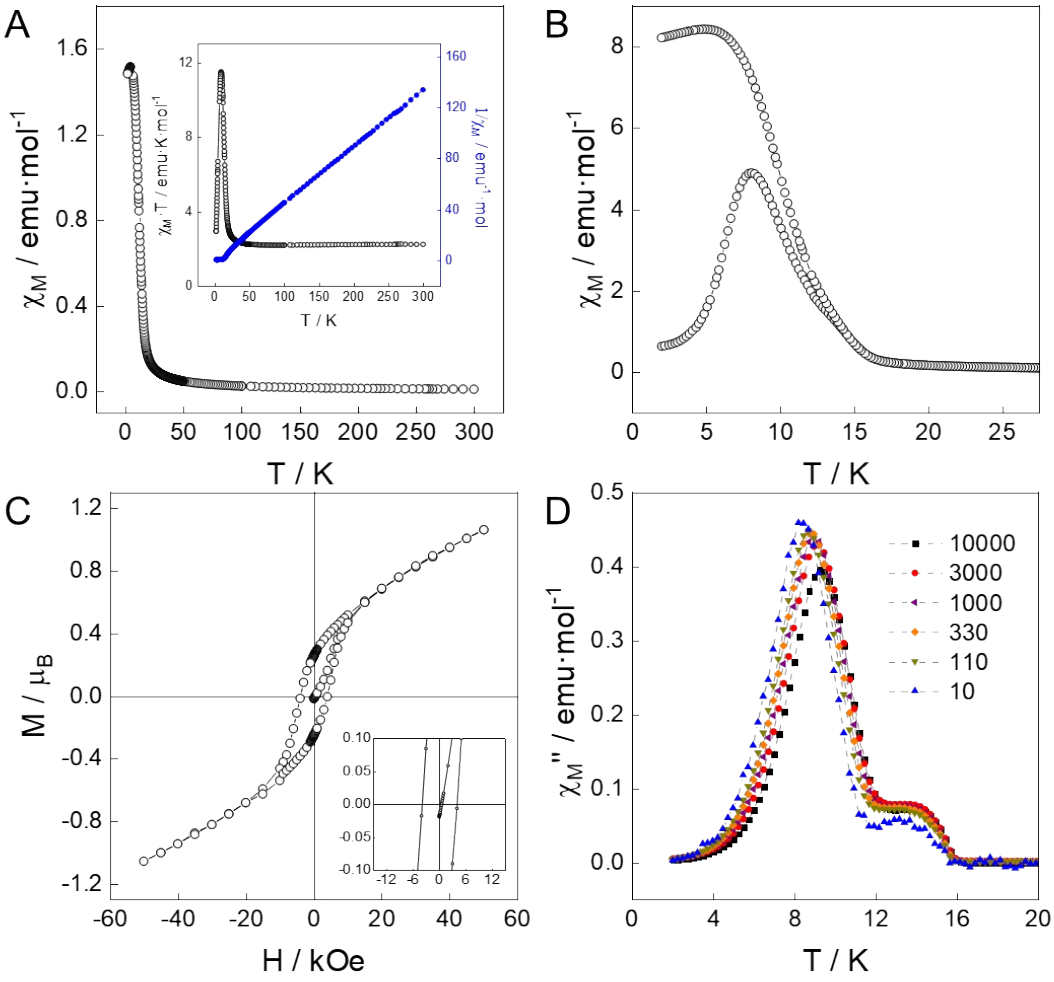

Figure S7. Magnetic properties of the NiFe-OS sample. (A) χM vs. T with an external applied field of 1000 Oe. The inset represents the thermal dependence of χM·T and the fitting of the χM-1 to a Curie–Weiss law; (B) FC/ZFC with an external applied field of 100 Oe. (C) Hysteresis cycle at 2 K. The inset shows a zoom of the low field region; (D) frequency dependence with the temperature for the out-of-phase (χM") signals at 10, 110, 330, 1000, 3000 and 100000 Hz.

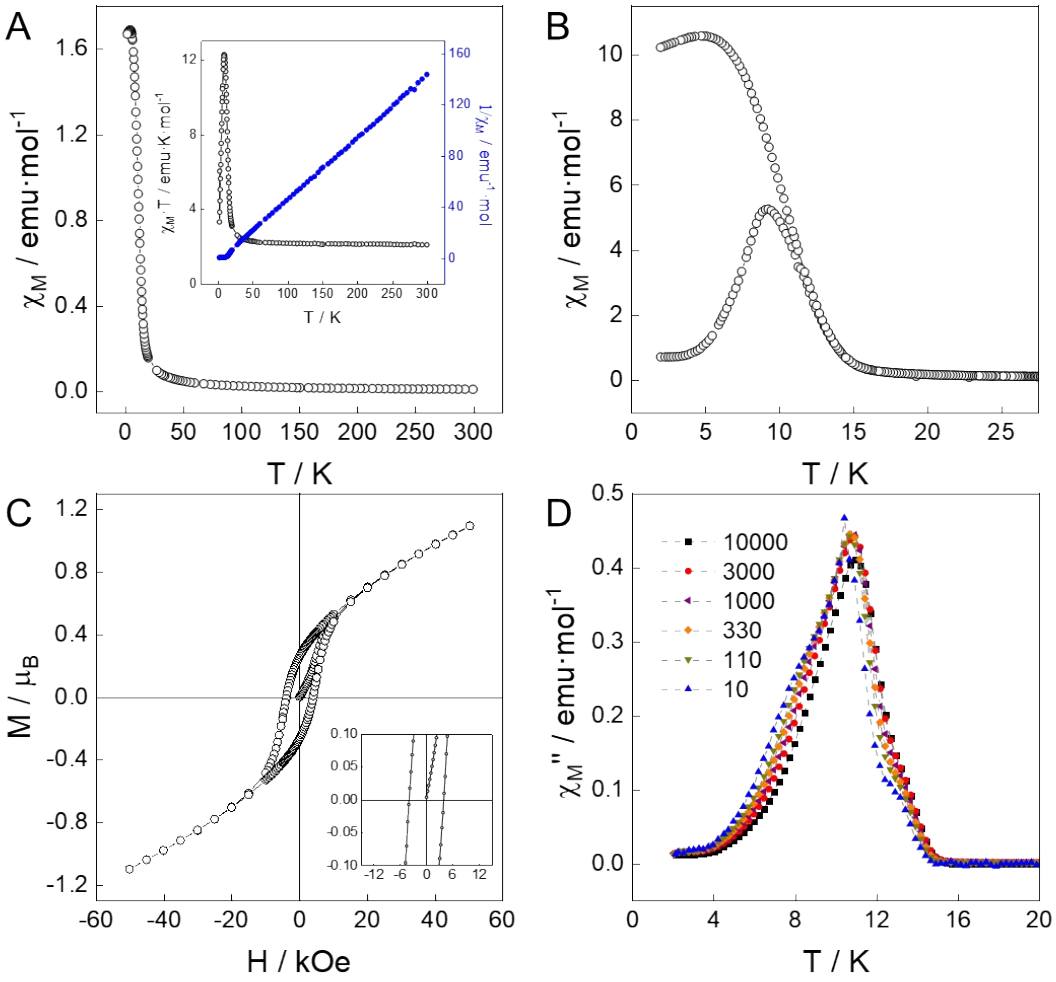

Figure S8. Magnetic properties of the NiFe-DS sample. (A) χM vs. T with an external applied field of 1000 Oe. The inset represents the thermal dependence of χM·T and the fitting of the χM-1 to a Curie–Weiss law; (B) FC/ZFC with an external applied field of 100 Oe. (C) Hysteresis cycle at 2 K. The inset shows a zoom of the low field region; (D) frequency dependence with the temperature for the out-of-phase (χM") signals at 10, 110, 330, 1000, 3000 and 100000 Hz.

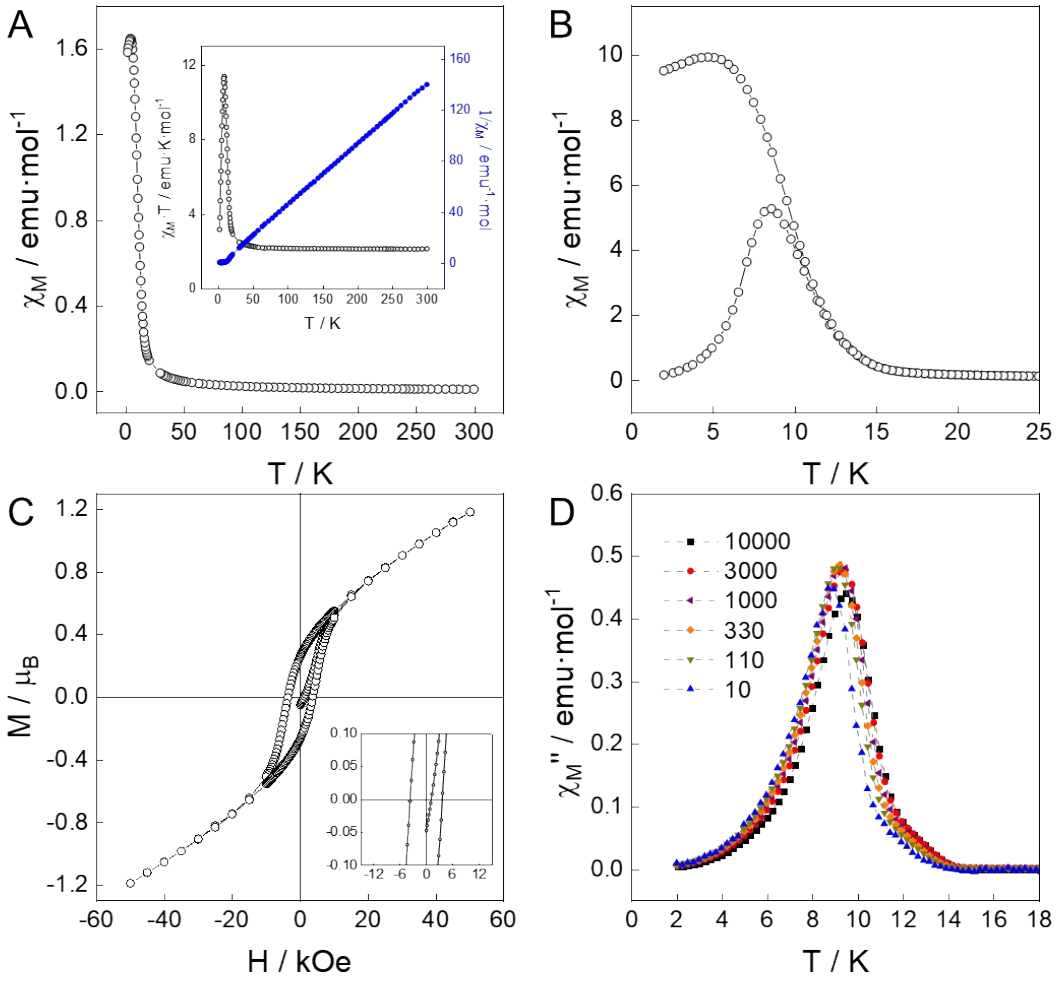

Figure S9. Magnetic properties of the NiFe-HDS sample. (A) χM vs. T with an external applied field of 1000 Oe. The inset represents the thermal dependence of χM·T and the fitting of the χM-1 to a Curie–Weiss law; (B) FC/ZFC with an external applied field of 100 Oe. (C) Hysteresis cycle at 2 K. The inset shows a zoom of the low field region; (D) frequency dependence with the temperature for the out-of-phase (χM") signals at 10, 110, 330, 1000, 3000 and 100000 Hz.

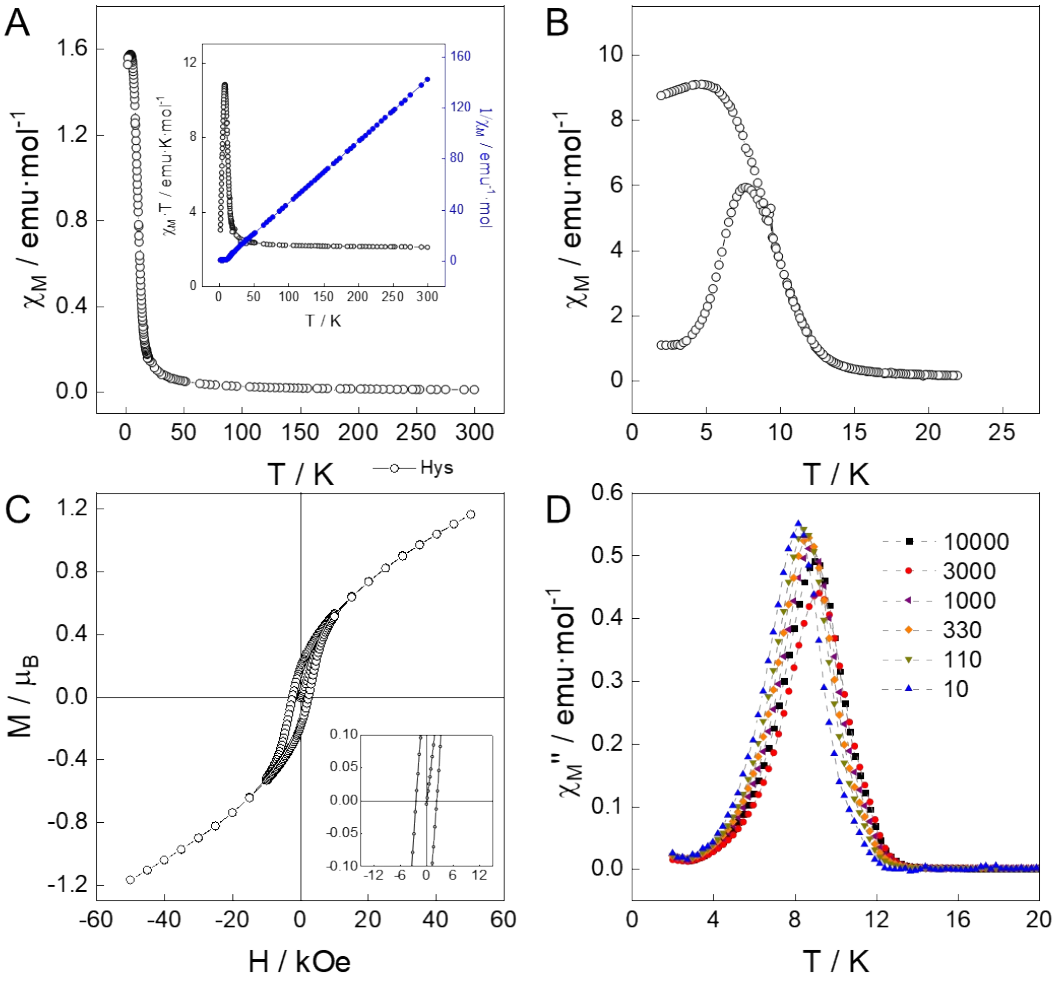

Figure S10. Magnetic properties of the NiFe-ODS sample. (A) χ_M vs. T with an external applied field of 1000 Oe. The inset represents the thermal dependence of χ_M·T and the fitting of the χ_M^{-1} to a Curie–Weiss law; (B) FC/ZFC with an external applied field of 100 Oe. (C) Hysteresis cycle at 2 K. The inset shows a zoom of the low field region; (D) frequency dependence with the temperature for the out-of-phase (χ_M'') signals at 10, 110, 330, 1000, 3000 and 100000 Hz.

Table S2. Probability P(m) of finding *m* Ni^{II} nearest neighbours of Fe^{III} according to the binomial distribution (eq.[1])

compound	*y*	P(6)	P(5)	P(4)	P(3)	P(2)	P(m≤1)
NiFe-Cl	2.7	0.152	0.337	0.310	0.152	0.042	<0.007
NiFe-ODS	2.8	0.164	0.346	0.304	0.142	0.038	<0.006

Table S3. Sextet relative areas *I*(*m*) expected for a completely random cation distribution

compound	I(6)	I(5)	I(4)	I(*m*≤3)	-
NiFe-Cl	15%	34%	31%	20%	-
NiFe-ODS	16%	35%	30%	19%	

Table S4. Estimated parameters from the Mössbauer spectra taken at different temperatures

sample	Ni:Fe d	T	IS	QS	B_{hf}	I (%)	$<B_{hf}>$
NiFe - Cl	2.7	295 K	0.35	0.51	-	100	
NiFe - Cl	7.8 Å	4 K	0.48	0.44	52.9	55	
			0.47	0.30	50.3	21	50.7
			0.47	0.17	47.4	15	
			0.45	0.12	44.0	9	
NiFe - ODS	2.8	295K	0.35	0.52	-	100	
NiFe - ODS	32 Å	4K	0.48	0.39	52.4	41	
			0.49	0.20	49.8	26	49.5
			0.47	0.17	47.0	20	
			0.47	0.11	43.3	13	

d interlamellar spacing

IS (mm/s) isomer shift relative to metallic α-Fe at 295 K; QS (mm/s) average quadrupole splitting estimated for distribution of quadrupole doublets; ε (mm/s) quadrupole shift estimated for magnetic sextets. B_{hf} (tesla) magnetic hyperfine field; *I* relative areas. Estimated errors $\leq$ 0.02 mm/s for IS, QS, ε, < 0.2 T for B_{hf} and <2% for I.

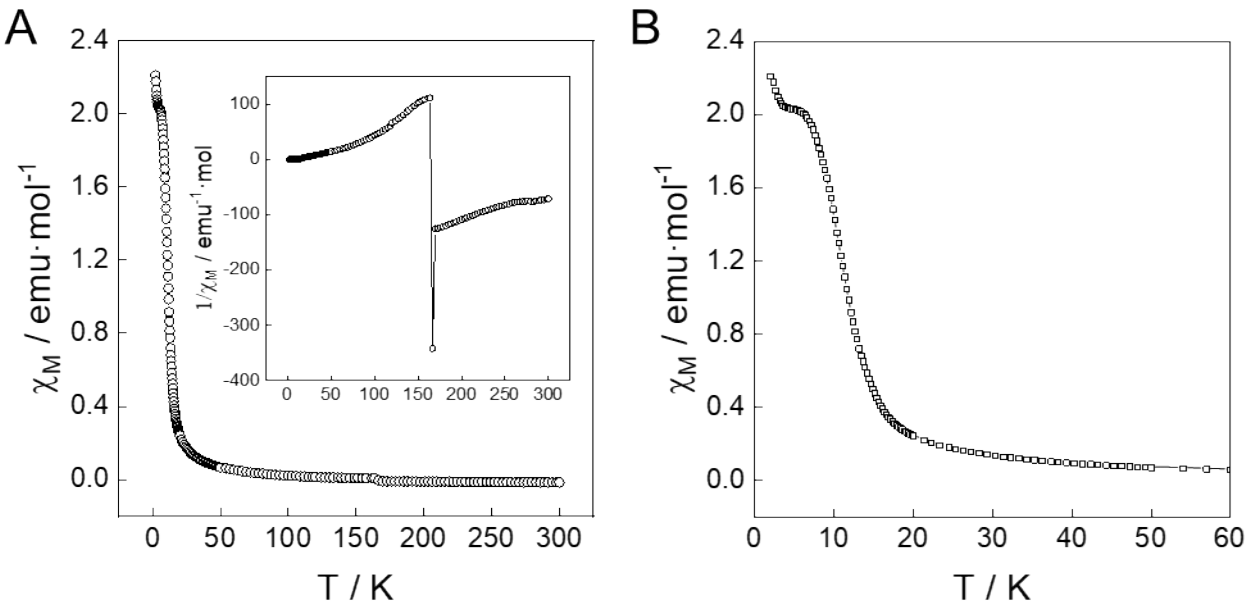

Figure S12. χ_M vs. T with an external applied field of 1000 Oe for NiFe-Cl exfoliated in formamide.

1 L.-J. Zhou, X. Huang, H. Chen, P. Jin, G.-D. Li and X. Zou, *Dalton Transactions*, 2015, **44**, 11592–11600.
2 L. Dang, H. Liang, J. Zhuo, B. K. Lamb, H. Sheng, Y. Yang and S. Jin, *Chemistry of Materials*, 2018, **30**, 4321–4330.
3 J. A. Carrasco, S. Cardona-Serra, J. M. Clemente-Juan, A. Gaita-Ariño, G. Abellán and E. Coronado, *Inorganic Chemistry*, 2018, **57**, 2013–2022.
4 J. W. Lee, W. C. Choi and J.-D. Kim, *CrystEngComm*, 2010, **12**, 3249.
5 R. B. Viana, A. B. F. da Silva and A. S. Pimentel, *Advances in Physical Chemistry*, 2012, **2012**, 1–14.